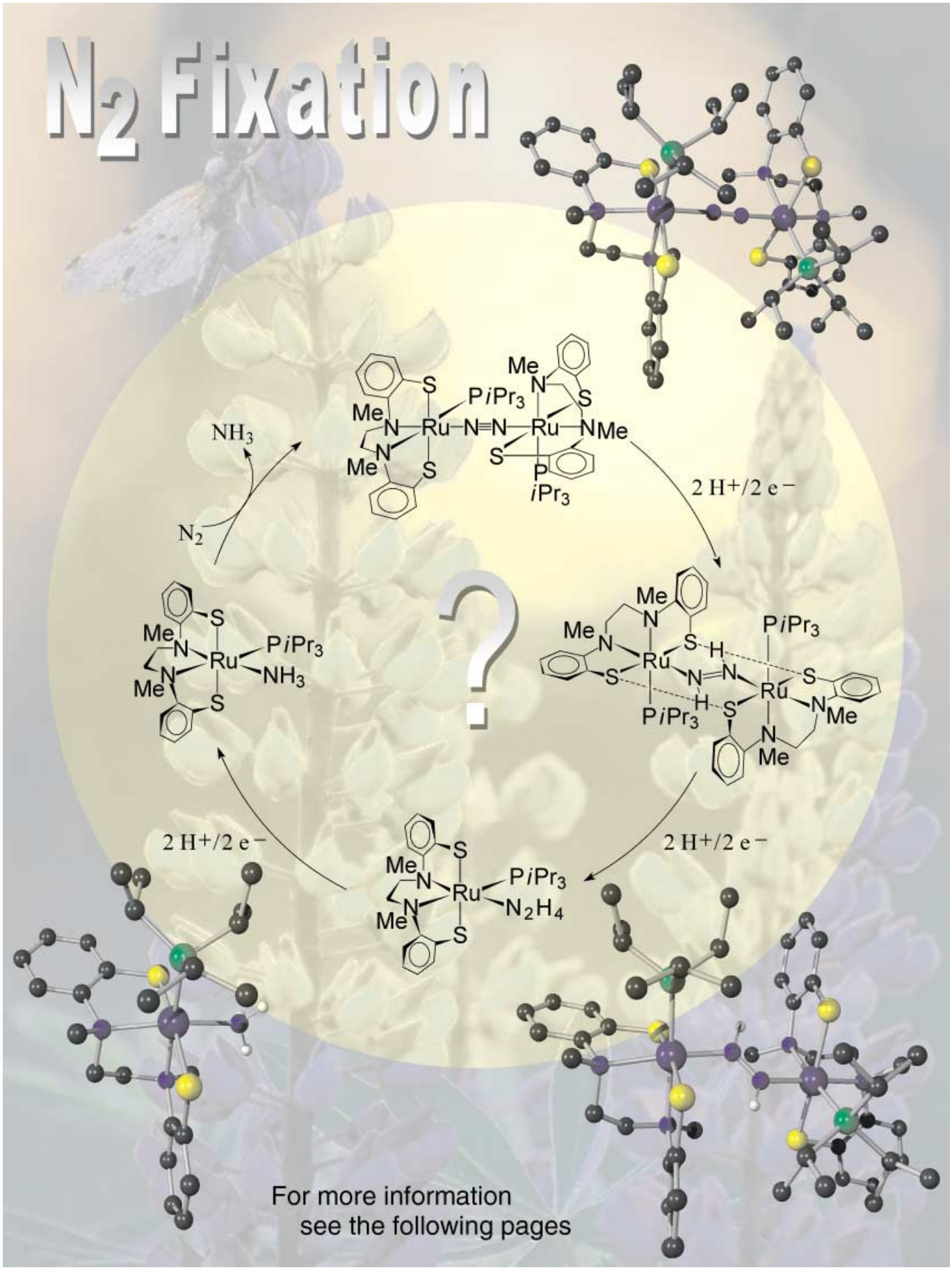

 DOI: 10.1002/chem.200305499

Binding N_2, N_2H_2, N_2H_4, and NH_3 to Transition-Metal Sulfur Sites: Modeling Potential Intermediates of Biological N_2 Fixation[+]

Dieter Sellmann,†[a] A. Hille,*[a] A. Rösler,[a] F. W. Heinemann,[a] M. Moll,[a] G. Brehm,[b] S. Schneider,[b] M. Reiher,[c] B. A. Hess,[c] and W. Bauer[d]

Abstract: In the quest for low-molecular-weight metal sulfur complexes that bind nitrogenase-relevant small molecules and can serve as model complexes for nitrogenase, compounds with the [Ru(P*i*Pr$_3$)('$N_2Me_2S_2$')] fragment were found ('$N_2Me_2S_2$'$^{2-}$ = 1,2-ethanediamine-*N*,*N*′-dimethyl-*N*,*N*′-bis(2-benzenethiolate)$^{2-}$). This fragment enabled the synthesis of a first series of chiral metal sulfur complexes, [Ru(L)(P*i*Pr$_3$)('$N_2Me_2S_2$')] with L = N_2, N_2H_2, N_2H_4, and NH_3, that meet the biological constraint of forming under mild conditions. The reaction of [Ru(NCCH$_3$)(P*i*Pr$_3$)('$N_2Me_2S_2$')] (**1**) with NH_3 gave the ammonia complex [Ru(NH$_3$)(P*i*Pr$_3$)('$N_2Me_2S_2$')] (**4**), which readily exchanged NH_3 for N_2 to yield the mononuclear dinitrogen complex [Ru(N_2)(P*i*Pr$_3$)('$N_2Me_2S_2$')] (**2**) in almost quantitative yield. Complex **2**, obtained by this new efficient synthesis, was the starting material for the synthesis of dinuclear (*R*,*R*)- and (*S*,*S*)-[μ-N_2{Ru(P*i*Pr$_3$)('$N_2Me_2S_2$')}$_2$] ((*R*,*R*)-/(*S*,*S*)-**3**). (Both **2** and **3** have been reported previously.) The as-yet inexplicable behavior of complex **3** to form also the *R*,*S* isomer in solution has been revealed by DFT calculations and ^{2}D NMR spectroscopy studies. The reaction of **1** or **2** with anhydrous hydrazine yielded the hydrazine complex [Ru(N_2H_4)(P*i*Pr$_3$)('$N_2Me_2S_2$')] (**6**), which is a highly reactive intermediate. Disproportionation of **6** resulted in the formation of mononuclear diazene complexes, the ammonia complex **4**, and finally the dinuclear diazene complex [μ-N_2H_2{Ru(P*i*Pr$_3$)('$N_2Me_2S_2$')}$_2$] (**5**). Dinuclear complex **5** could also be obtained directly in an independent synthesis from **1** and N_2H_2, which was generated in situ by acidolysis of $K_2N_2(CO_2)_2$. Treatment of **6** with CH_2Cl_2, however, formed a chloromethylated diazene species [{Ru(P*i*Pr$_3$)('$N_2Me_2S_2$')}-μ-N_2H_2{Ru(Cl)('$N_2Me_2S_2CH_2Cl$')}] (**9**) ('$N_2Me_2S_2CH_2Cl$'$^{2-}$ = 1,2-ethanediamine-*N*,*N*′-dimethyl-*N*-(2-benzenethiolate)$^{1-}$-*N*′-(2-benzenechloromethylthioether)$^{1-}$]. The molecular structures of **4**, **5**, and **9** were determined by X-ray crystal structure analysis, and the labile N_2H_4 complex **6** was characterized by NMR spectroscopy.

Keywords: enzyme models · nitrogen fixation · ruthenium · S ligands

[a] Prof. Dr. D. Sellmann,† Dr. A. Hille, Dr. A. Rösler, Dr. F. W. Heinemann, Dr. M. Moll
Institut für Anorganische Chemie
der Universität Erlangen-Nürnberg
Egerlandstrasse 1, 91058 Erlangen (Germany)
Fax: (+49) 9131-857367
E-mail: hille@anorganik.chemie.uni-erlangen.de

[b] Dr. G. Brehm, Prof. Dr. S. Schneider
Institut für Physikalische Chemie
der Universität Erlangen-Nürnberg
Egerlandstrasse 3, 91058 Erlangen (Germany)

[c] Priv.-Doz. Dr. M. Reiher, Prof. Dr. B. A. Hess
Institut für Theoretische Chemie
der Universität Erlangen-Nürnberg
Egerlandstrasse 3, 91058 Erlangen (Germany)

[d] Priv.-Doz. Dr. W. Bauer
Institut für Organische Chemie
der Universität Erlangen-Nürnberg
Henkestrasse 42, 91054 Erlangen (Germany)

[†] Died on May 6, 2003.

[+] Transition-Metal Complexes with Sulfur Ligands, Part 161. For Part 160, see: D. Sellmann, R. Prakash, F. W. Heinemann, *Eur. J. Inorg. Chem.*, in press.

Introduction

In spite of long-lasting efforts, including the X-ray crystal structure determination of FeMo nitrogenase and its metal sulfur cofactors (FeMoco), the mechanism of biological N_2 fixation has remained poorly understood.[1] In the search for model complexes for nitrogenase, transition-metal species with ancillary sulfur ligands that can bind molecular nitrogen to give N_2 complexes are a primary target, because the first step of biological N_2 fixation is agreed to involve coordination of N_2 to the FeMo cofactors resulting in adducts that represent mono-, di-, or polynuclear transition-metal sulfur complexes.[2] Model complexes which catalyze the reduction of N_2 under nitrogenase-relevant conditions are still unknown.[3] Numerous findings indicate that the N_2 ligand of these complexes is subsequently reduced by coupled [$2H^+/2e^-$] reduction steps via diazene and hydrazine species to ammonia.[4]

DOI: 10.1002/chem.200305499

In order to investigate the nature of this reduction process, N_2 complexes with transition-metal sulfur cores that form from N_2 and metal sulfur complex precursors without the use of abiologically strong reductants (for example, alkaline metals) are indispensable prerequisites. However, the only complexes known so far that meet the aforementioned requirements are the ruthenium complexes [Ru(N_2)(P*i*Pr$_3$)('$N_2Me_2S_2$')] and [μ-N_2{Ru(P*i*Pr$_3$)('$N_2Me_2S_2$')}$_2$] ('$N_2Me_2S_2$'$^{2-}$ = 1,2-ethanediamine-*N*,*N*′-dimethyl-*N*,*N*′-bis(2-benzenethiolate)$^{2-}$).[5,6] Their as-yet hypothetical reduction by [2H$^+$/2e$^-$] transfer steps is anticipated to give the corresponding diazene, hydrazine, and finally ammonia complexes. In order to explore the viability of these potential reduction intermediates, attempts were made for their synthesis, starting from hydrazine, ammonia, and other nitrogenous compounds. This paper describes, inter alia, the first series of complexes in which N_2, N_2H_2, N_2H_4, and NH_3 bind to identical transition-metal sulfur complex fragments.

Results and Discussion

N_2 and NH_3 complexes: In a previously reported synthesis the mononuclear N_2 complex [Ru(N_2)(P*i*Pr$_3$)('$N_2Me_2S_2$')] (**2**) was obtained by replacing the labile CH_3CN ligand in [Ru(NCCH$_3$)(P*i*Pr$_3$)('$N_2Me_2S_2$')] (**1**) by molecular nitrogen under ambient conditions according to Scheme 1.[5,6] Lower-

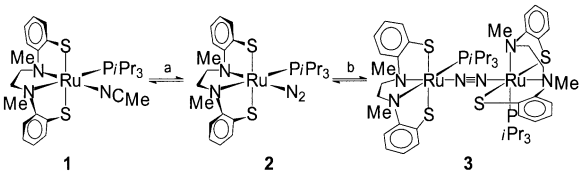

1 2 3

Scheme 1. Synthesis of [Ru(N_2)(P*i*Pr$_3$)('$N_2Me_2S_2$')] (**2**) and [μ-N_2{Ru(P*i*Pr$_3$)('$N_2Me_2S_2$')}$_2$] (**3**) from [Ru(NCCH$_3$)(P*i*Pr$_3$)('$N_2Me_2S_2$')] (**1**). a) +/− N_2, +/− CH_3CN, toluene, 50–60 °C; b) +/− N_2, toluene, 50 °C.

ing the N_2 pressure by passing a stream of argon through a solution of mononuclear **2** resulted in partial removal of the N_2 ligand and subsequent formation of dinuclear [μ-N_2{Ru(P*i*Pr$_3$)('$N_2Me_2S_2$')}$_2$] (**3**). As indicated, the reactions were reversible. The N_2 complexes **2** and **3** could be completely characterized.

As a consequence of the reversibility of the first exchange step the isolation of pure **2** was difficult. The CH_3CN/N_2 exchange could never be driven to completeness, and the remaining acetonitrile complex **1** had to be separated from the N_2 complex **2** by elaborate washing and recrystallization procedures. Therefore, a better precursor for the synthesis of **2** (and **3**) was desirable and was finally found in the corresponding ammonia complex [Ru(NH_3)(P*i*Pr$_3$)('$N_2Me_2S_2$')] (**4**). Beyond that, the NH_3 complex represents the final product in the as-yet hypothetical reduction of either **2** or **3**. The NH_3 complex **4** was obtained by passing a stream of gaseous NH_3 through a tetrahydrofuran (THF) solution of [Ru(NCCH$_3$)(P*i*Pr$_3$)('$N_2Me_2S_2$')] (**1**) at slightly elevated temperature [Eq. (1)].

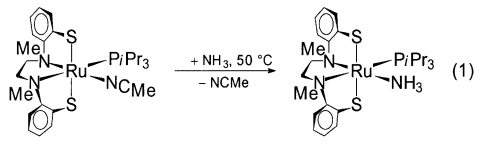

(1)

1 4

By use of **4** as a precursor, the reaction could now be driven to completeness and monitored by IR spectroscopy, which indicated a decrease of the ν(C≡N) band of **1** at 2246 cm^{-1}. [Ru(NH_3)(P*i*Pr$_3$)('$N_2Me_2S_2$')] (**4**) was isolated in approximately quantitative yield and forms dark orange crystals. The IR spectrum of complex **4** exhibits characteristic ν(N–H) bands at 3350, 3306, 3240, and 3166 cm^{-1}. A ^{31}P signal at δ = 56.94 ppm and the NH_3 proton signals at δ = 1.39 ppm are observed in the ^{31}P and ^{1}H NMR spectra, respectively. The molecular structure of **4** was determined by X-ray crystal structure analysis. The NH_3 ligand in **4** proved much more labile than the CH_3CN ligand in [Ru(NCCH$_3$)(P*i*Pr$_3$)('$N_2Me_2S_2$')] (**1**). Monitoring NH_3/N_2 exchange of **4** in toluene by IR spectroscopy revealed a considerably faster increase of the $\nu(N_2)$ band of **2** at 2115 cm^{-1}, and the reaction could be driven to completeness with a nearly quantitative yield of **2**, which could be obtained in only 46 % yield when starting from **1**.

N_2H_4 and N_2H_2 complexes: Addition of excess anhydrous N_2H_4 to a light-green THF solution of [Ru(NCCH$_3$)(P*i*Pr$_3$)('$N_2Me_2S_2$')] (**1**) resulted in a color change to deep yellow within a few minutes. Within the course of 4–6 h the solution turned deep blue and a blue solid started to precipitate. Addition of MeOH completed the precipitation of the solid, which was isolated in 68 % yield (based on **1**) and characterized as the diazene complex [μ-N_2H_2{Ru(P*i*Pr$_3$)('$N_2Me_2S_2$')}$_2$] (**5**; see below) [Eq. (2)].

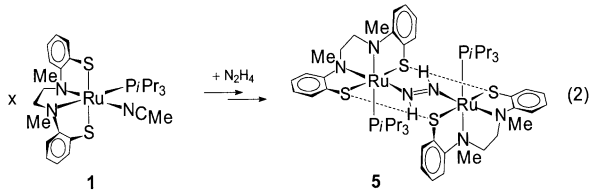

(2)

1 5

The blue color of **5** is characteristic for [Ru–NH=NH–Ru] chromophores.[7] A singlet at δ = −13.61 ppm in the ^{1}H NMR spectrum indicated the presence of the diazene ligand and a two-fold symmetry of **5**.[8] Its molecular structure could be determined by X-ray crystal structure analysis.

This unexpected result prompted us to look for a more direct and rational synthesis of **5**. The diazene complex **5** also formed when [Ru(NCCH$_3$)(P*i*Pr$_3$)('$N_2Me_2S_2$')] (**1**) was treated with diazene that was generated in situ by acidolysis of $K_2N_2(CO_2)_2$ with acetic acid [Eq. (3)].[9] Dropwise addition of a dilute aqueous solution of acetic acid to a solution of **1** and suspended solid $K_2N_2(CO_2)_2$ in THF liberated the highly reactive diazene molecule HN=NH[10] (ΔH_f = +212 kJ mol^{-1}), which reacted with **1** to give [μ-N_2H_2{Ru(P*i*Pr$_3$)('$N_2Me_2S_2$')}$_2$] (**5**). Removal of the aqueous phase and

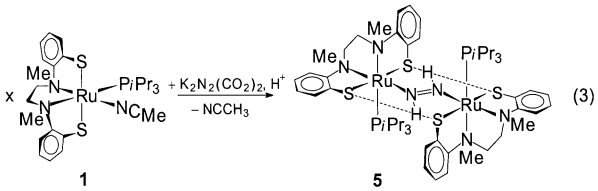

addition of MeOH to the THF phase led to the precipitation of blue microcrystals of **5**, which were obtained in yields of approximately 46% (based on **1**).

The diazene complex **5** also formed when the N_2 complex **2** was treated with N_2H_4 in [D_8]THF. Monitoring this reaction by ^{31}P and ^1H NMR spectroscopy (Figure 1) provided

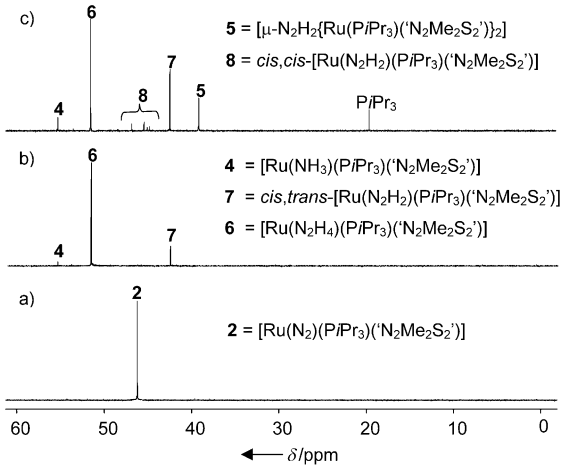

Figure 1. Monitoring the formation of [μ-N_2H_2{Ru(P*i*Pr$_3$)('$N_2Me_2S_2$')}$_2$] (**5**) by ^{31}P NMR spectroscopy in [D_8]THF. a) [Ru(N_2)(P*i*Pr$_3$)('$N_2Me_2S_2$')] (**2**); b) + excess N_2H_4 after 10 min; c) + excess N_2H_4 after 4 h.

deeper insight into the reaction pathways leading to **5**. Figure 1a shows the ^{31}P NMR spectrum of the N_2 complex **2**. After addition of 6–8 equivalents of N_2H_4, the ^{31}P NMR signal of **2** disappeared and three new signals at $\delta = 56.92$, 53.09, and 43.95 ppm resulted (Figure 1b). The assignment of the signals shown in the figure is based on the ^1H NMR spectroscopic experiments (see below). After 4 h, the ^{31}P NMR spectrum showed additional signals, including liberated P*i*Pr$_3$ (Figure 1c). The assignment is again based on detailed analysis by ^1H NMR spectroscopy (see below).

The formation of the hydrazine complex [Ru(N_2H_4)(P*i*Pr$_3$)('$N_2Me_2S_2$')] (**6**; Figure 2) is indicated in the ^1H NMR spectrum by the two characteristic doublets at $\delta =$ 4.41 ppm (^2J(H,H) = 10.8 Hz, 1H, RuN**H**$_2$NH$_2$) and $\delta =$ 4.18 ppm (^2J(H,H) = 10.8 Hz, 1H, RuN**H**$_2$NH$_2$) for the metal-bound NH_2 group. A broad signal, which was assigned to the terminal NH_2 group, appeared at $\delta = 3.58$ ppm and was superimposed with the solvent signal. At −20 °C, this signal was shifted low-field to $\delta = 3.63$ ppm. Weak cross-peaks to the metal-bound NH_2 group were found in the ^1H-COSY spectrum and clearly defined the formation of [Ru(N_2H_4)(P*i*Pr$_3$)('$N_2Me_2S_2$')] (**6**).

In agreement with the ^{31}P NMR spectrum (Figure 1b), the ^1H NMR spectrum of the products obtained indicated the

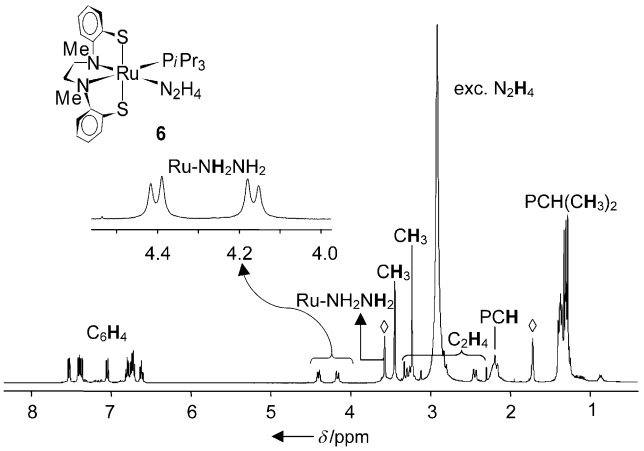

Figure 2. ^1H NMR spectrum of [Ru(N_2H_4)(P*i*Pr$_3$)('$N_2Me_2S_2$')] (**6**) in [D_8]THF, ◇ = [D_8]THF signals.

formation of two additional complexes. A singlet at $\delta =$ 1.39 ppm was assigned to the protons of coordinated NH_3 and indicated the ammonia complex [Ru(NH_3)(P*i*Pr$_3$)('$N_2Me_2S_2$')] (**4**) as another product. The low-field shift and coupling constants of two doublets at $\delta = 16.82$ and 16.15 ppm (^3J(H,H) = 28.0 Hz) were indicative for the formation of a mononuclear diazene complex *cis*,*trans*-[Ru(N_2H_2)(P*i*Pr$_3$)('$N_2Me_2S_2$')] (**7**) with a *trans* diazene ligand.[8,11] The splitting into doublets is due to coupling of the inequivalent protons of the terminal diazene ligand in the Ru–NH=NH entity. Comparable shifts and coupling constants were found in heterodinuclear [$(OC)_5Cr{-}N_2H_2{-}Mn(CO)_2Cp$] and mononuclear complexes of the type [M(N_2H_2)$(CO)_2(PPh_3)_2$Br]SO_3CF_3 (Cp = cyclopentyl, M = Ru, Os).[12] In addition, the ^1H NMR spectrum indicated that the '$N_2Me_2S_2$' ligand in **7** adopted a regular *cis*,*trans* arrangement (see below).

Since no additional oxidants or reductants were present, the formation of mononuclear NH_3 and N_2H_2 complexes is rationalized best by a disproportionation ($2\,N_2H_4 \rightarrow N_2H_2 + 2\,NH_3$) of the hydrazine complex [Ru(N_2H_4)(P*i*Pr$_3$)('$N_2Me_2S_2$')] (**6**) into mononuclear N_2H_2 and NH_3 complexes **7** and **4** [Eq. (4)]. Upon coordination to the elec-

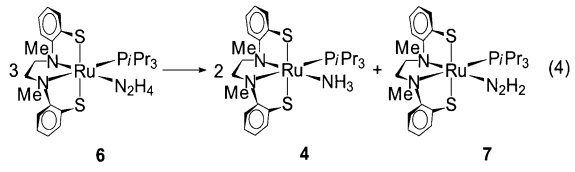

tron-rich [Ru(P*i*Pr$_3$)('$N_2Me_2S_2$')] fragment, the N_2H_4 ligand in **6** is highly activated, a fact resulting in the described disproportionation.

In the course of 4–6 h, 4 additional low-field-shifted signals showing a splitting pattern similar to the mononuclear diazene complex **7** were observed. These doublets were assigned to the formation of further mononuclear diazene complexes **8** (Figure 3). Finally, a low-field-shifted singlet at $\delta = 13.61$ ppm indicated the formation of the C_2-symmetric dinuclear diazene complex [μ-N_2H_2{Ru(P*i*Pr$_3$)('$N_2Me_2S_2$')}$_2$]

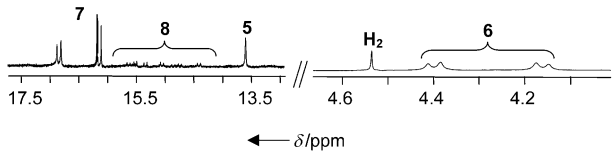

Figure 3. Diazene and hydrazine NH signals of **5**, **6**, **7**, and **8** in the ^{1}H NMR spectrum.

(**5**). In addition, the formation of free H_2 was observed, indicated by a strong signal at $\delta = 4.54$ ppm. This free H_2 possibly results from the decomposition of either free N_2H_4 or coordinated N_2H_2 into N_2 and H_2.

The appearance of at least four different mononuclear diazene complexes **8**, presumably with the identical formula [Ru(N_2H_2)(P*i*Pr$_3$)('$N_2Me_2S_2$')], is rationalized by the fact that 1) N_2H_2 ligands in transition-metal thiolate complexes form comparably strong hydrogen bonds to the thiolate donors, which can result in a total hydrogen-bond energy of up to 21 kJ mol^{-1},[13] 2) chiral *cis*,*trans*-[Ru(N_2H_2)(P*i*Pr$_3$)('$N_2Me_2S_2$')] can form two different hydrogen-bond species **I** and **II**, which are diastereomers because the Ru center is stereogenic,[14] and 3) the [Ru(P*i*Pr$_3$)('$N_2Me_2S_2$')] fragment itself can also exist in the *cis*,*cis* configurations **III** and **IV**, which are diastereomeric both to each other and to the fragments in **I** and **II** (Scheme 2).[15] The two diastereomers **III** and **IV** can again each give rise to two hydrogen-bond diastereomers when diazene ligands are present.

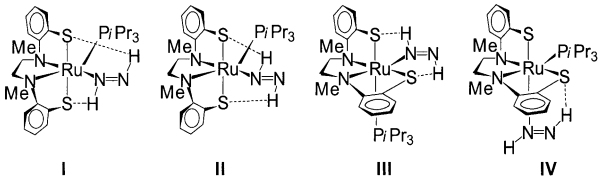

Scheme 2. Hydrogen-bond *cis*,*trans* and *cis*,*cis* stereoisomers of [Ru(N_2H_2)(P*i*Pr$_3$)('$N_2Me_2S_2$')].

The formation of *cis*,*cis* isomers requires the rearrangement of the '$N_2Me_2S_2$'$^{2-}$ ligand within the [Ru('$N_2Me_2S_2$')] core. This can only take place when five-coordinate intermediates are involved, for example, fragments of the [Ru(L)('$N_2Me_2S_2$')] type that have lost either the phosphane or the nitrogenous co-ligand. The occurrence of free P*i*Pr$_3$ (Figure 1c) is indicative for the formation of such five-coordinate fragments, which can give rise to *cis*,*cis*-[Ru(L)(P*i*Pr$_3$)('$N_2Me_2S_2$')] complexes [Eq. (5)] with ligands like $NCCH_3$, NH_3, N_2H_2, or N_2H_4.

However, *cis*,*cis* configuration of the '$N_2Me_2S_2$'$^{2-}$ ligand is usually not favored, unless sterical constraints enforce this less-common coordination mode. Diazene ligands, which are capable of forming strong hydrogen bridges to neighboring S(thiolate) functions (see above), can impose such steric constraints and therefore promote the formation of *cis*,*cis*-[Ru(N_2H_2)(P*i*Pr$_3$)('$N_2Me_2S_2$')] (**8**) complexes. Similar to the findings for the mononuclear hydrazine complex **6**, the mononuclear diazene complexes **7** and **8** also turned out to be short-lived species. ^{31}P and ^{1}H NMR spectra that were recorded from the reaction solutions of **1** with N_2H_4 after one week indicated that practically all mononuclear diazene complexes and the hydrazine complex had disappeared. This may explain why all attempts to crystallize the complexes **6**, **7**, and **8**, were unsuccessful.

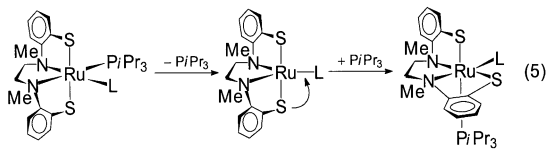

The final formation of the dinuclear diazene complex **5**, which is probably the least soluble and most stable one of all these complexes, is rationalized by the reaction of, most probably, the *cis*,*trans*-configured N_2H_2 complex [Ru(N_2H_2)(P*i*Pr$_3$)('$N_2Me_2S_2$')] (**7**) with [Ru(NH_3)(P*i*Pr$_3$)('$N_2Me_2S_2$')] (**4**), whose NH_3 ligand is, as described above, extremely labile and can easily be replaced by the terminal NH group of the mononuclear diazene species. This reaction pathway is shown in Equation (6).

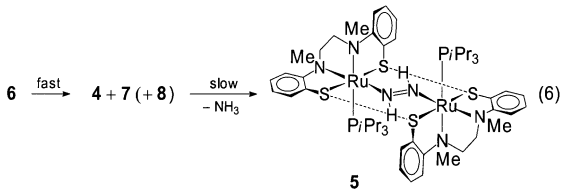

Formation of thiolate-bridged dimeric complexes: Upon decoordination of the P*i*Pr$_3$ co-ligand, five-coordinate fragments [Ru(L)('$N_2Me_2S_2$')] form, which can also give rise to dimerization reactions. As a consequence of the loss of the bulky phosphane co-ligand, the formation of sparingly soluble, thiolate-bridged complexes of the general formula [{Ru(L)('$N_2Me_2S_2$')}$_2$] can be expected [Eq. (7)].

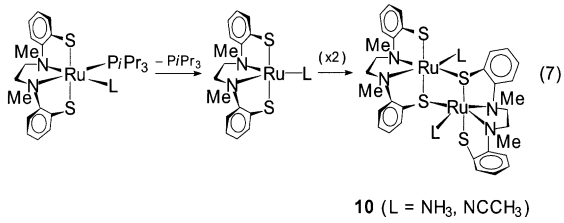

The viability of these thiolate-bridged complexes is demonstrated by the isolation of [{Ru($NCCH_3$)$_{0.8}$(NH_3)$_{0.2}$('$N_2Me_2S_2$')}$_2$] (**10**), which precipitated from mother liquors of the reaction of **1** with N_2H_4 within two months. The exclusive formation and the unusual stoichiometry found for complex **10** may be rationalized as follows. The dimerization of five-coordinate [Ru(L)('$N_2Me_2S_2$')] fragments with terminal N_2H_2, N_2H_4, and NH_3 ligands (L) can, in general, result in all possible combinations of these ligands in the dinuclear, thiolate-bridged [{Ru(L)('$N_2Me_2S_2$')}$_2$] complexes, for example, in [{Ru-

$(N_2H_2)(\text{'}N_2Me_2S_2\text{'})\}\{Ru(N_2H_4)(\text{'}N_2Me_2S_2\text{'})\}]$ or $[\{Ru(N_2H_2)(\text{'}N_2Me_2S_2\text{'})\}\{Ru(NH_3)(\text{'}N_2Me_2S_2\text{'})\}]$. With regard to the ligands mentioned above, only NH_3 is stable. The decomposition of the N_2H_2 and N_2H_4 ligands (see above) generates free coordination sites which can be occupied by CH_3CN ligands. At this point, it has to be stressed that the mother liquors from the reaction of the acetonitrile complex $[Ru(NCCH_3)(PiPr_3)(\text{'}N_2Me_2S_2\text{'})]$ (**1**) with hydrazine contain comparably high quantities of liberated CH_3CN.

Chloromethylation of $[\mu\text{-}N_2H_2\{Ru(PiPr_3)(\text{'}N_2Me_2S_2\text{'})\}_2]$ (5): The high reactivity of all the species described above also became evident when recrystallization of the diazene complex $[\mu\text{-}N_2H_2\{Ru(PiPr_3)(\text{'}N_2Me_2S_2\text{'})\}_2]$ (**5**) was attempted with CH_2Cl_2 instead of a MeOH/THF mixture. This precedure resulted in the formation of a chloromethylated diazene complex, namely $[\{Ru(PiPr_3)(\text{'}N_2Me_2S_2\text{'})\}\text{-}\mu\text{-}N_2H_2\{Ru(Cl)(\text{'}N_2Me_2S_2CH_2Cl\text{'})\}]$ (**9**) [Eq. (8)].

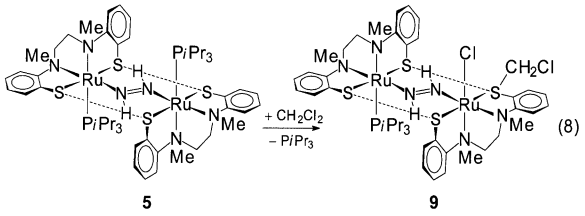

In order to elucidate the reaction pathway leading to the formation of **9**, the reaction was monitored by NMR spectroscopy in CD_2Cl_2. The ^1H and ^{31}P NMR spectra both indicated the complete conversion of **5** into the chloromethylated diazene complex $[\{Ru(PiPr_3)(\text{'}N_2Me_2S_2\text{'})\}\text{-}\mu\text{-}N_2D_2\{Ru(Cl)(\text{'}N_2Me_2S_2CH_2Cl\text{'})\}]$ (deuterated **9**) within three days. A singlet for the N_2H_2 protons, which are isochronic, at $\delta = 15.54$ ppm in the ^1H NMR spectra and a singlet for the remaining $PiPr_3$ substituent at $\delta = 43.00$ ppm in the ^{31}P NMR spectra were indicative for the formation of complex **9**. Other chloromethylated species were not observed.

It was of considerable interest that the ^{31}P NMR spectrum of complex **5** in $[D_8]$THF also indicated liberated $PiPr_3$. This demonstrated that the dissociation of $PiPr_3$ ligands is not exclusively limited to mononuclear $[Ru(L)(PiPr_3)(\text{'}N_2Me_2S_2\text{'})]$ complexes but can also take place with dinuclear species like **5**. The interaction of CH_2Cl_2 (or CD_2Cl_2) with the five-coordinate entity in complex **5** results in the splitting of one C–Cl bond. The chloro ligand binds to the ruthenium center and one thiolate donor is chloromethylated. This reaction pathway rationalizes the formation of complex **9** and likewise explains the instability of other mononuclear $[Ru(L)(PiPr_3)(\text{'}N_2Me_2S_2\text{'})]$ complexes towards CH_2Cl_2. Further chloromethylation of the intact $[Ru(PiPr_3)(\text{'}N_2Me_2S_2\text{'})]$ entity in complex **9** was not observed.

X-ray crystal structure analysis: The crystal structures of the diazene and ammonia complexes **4**, **5**, and **9**, and of dinuclear $[\{Ru(NCCH_3)_{0.8}(NH_3)_{0.2}(\text{'}N_2Me_2S_2\text{'})\}_2]$ (**10**) could be elucidated by X-ray crystal structure analysis and compared with the structure of $[\mu\text{-}N_2\{Ru(PiPr_3)(\text{'}N_2Me_2S_2\text{'})\}_2]$ (**3**), which has been previously published and is included here for the sake of completeness.[6] Figure 4 depicts the molecular structures of the complexes **3**, **4**, **5**, **9**, and **10**. The ruthenium centers of all $[Ru(L)(PiPr_3)(\text{'}N_2Me_2S_2\text{'})]$ complexes exhibit pseudo-octahedral coordination and *trans* thiolate donors. Dinuclear **3** and **5** exhibit crystallographically required C_2 symmetry, **4** and **9** are C_1 symmetric, and **10** has C_i symmetry.

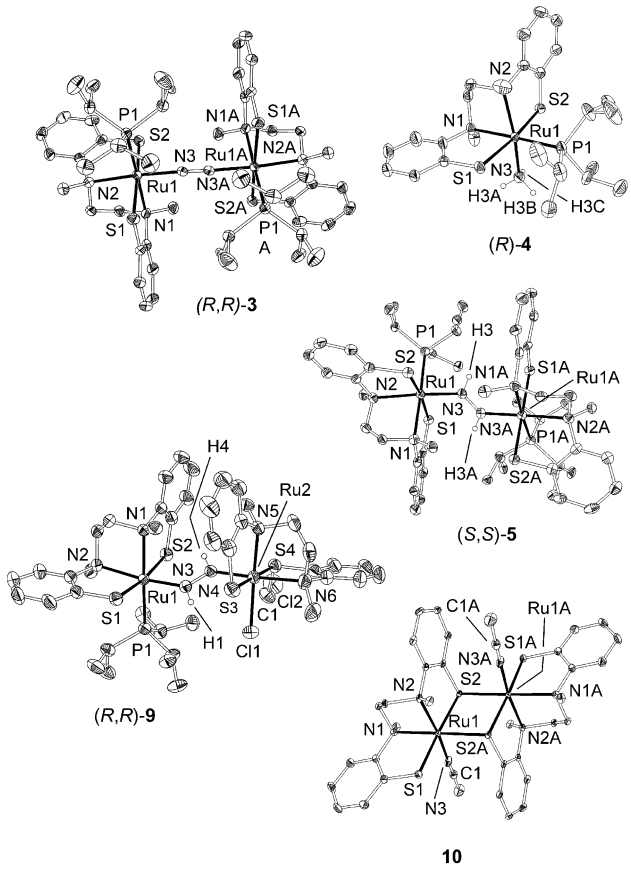

Figure 4. Molecular structures of (R,R)-$[\mu\text{-}N_2\{Ru(PiPr_3)(\text{'}N_2Me_2S_2\text{'})\}_2]$ ((*R*,*R*)-**3**), (*R*)-$[Ru(NH_3)(PiPr_3)(\text{'}N_2Me_2S_2\text{'})]$ ((*R*)-**4**), (S,S)-$[\mu\text{-}N_2H_2\{Ru(PiPr_3)(\text{'}N_2Me_2S_2\text{'})\}_2]$ ((*S*,*S*)-**5**), (R,R)-$[\{Ru(PiPr_3)(\text{'}N_2Me_2S_2\text{'})\}\text{-}\mu\text{-}N_2H_2\{Ru(Cl)(\text{'}N_2Me_2S_2CH_2Cl\text{'})\}]\cdot 1.5\,CH_2Cl_2$ ((*R*,*R*)-**9**$\cdot 1.5\,CH_2Cl_2$), and $[\{Ru(NCCH_3)_{0.8}(NH_3)_{0.2}(\text{'}N_2Me_2S_2\text{'})\}_2]$ (**10**) (50% probability ellipsoids; C-bound hydrogen atoms and solvent molecules omitted for clarity).

Table 1 lists selected bond distances and angles. All bond distances within the $[Ru(\text{'}N_2Me_2S_2\text{'})]$ cores of the complexes **3**, **4**, **5**, **9**, and **10** lie in the usual range. It is worth noting that the Ru1–N3 distances indicate multiple Ru–N bond character in **3** (195.7(3) pm), **5** (199.4(5) pm), and **9** (198.0(4) pm, for Ru1–N5) but single bond character in **4** (213.2(5) pm); this corresponds with the fact that N_2 and N_2H_2 are σ-donor–π-acceptor ligands, while NH_3 is a σ donor only.

These different ligand properties of N_2 and N_2H_2 versus those of NH_3 are also observed in the Ru1–N2 bonds *trans* to either the N_2, N_2H_2, or NH_3 ligands. The Ru1–N2 bond is shortest in **4** (221.4(2) pm) and longest in **5** (225.7(6) pm).

The observation that in these complexes the Ru1–N1 distances are longer than the Ru–N2 distances reflects the fact

Table 1. Selected bond lengths [pm] and angles [°] in **3**, **4**, **5**, **9**·1.5 CH_2Cl_2, and **10**.

	3	**4**	**5**	**9**[a]	**10**
Ru1–N1	228.7(4)	229.3(5)	232.0(6)	228.5(4)	219.6(2)
Ru1–N2	223.2(4)	221.4(5)	225.7(6)	223.6(4)	217.9(2)
Ru1–S1	238.5(2)	237.3(2)	236.6(2)	238.1(2)	236.0(1)
Ru1–S2	239.5(2)	238.5(2)	239.2(2)	236.0(2)	237.0(1)
Ru1–P1/S2A	237.9(2)	230.3(2)	236.1(2)	234.6(2)	241.8(1)
Ru1–N3	195.7(3)	213.2(5)	199.4(5)	198.0(4)	202.0(2)
N3–N3A/N4/C1	112.5(7)	–	127.0(1)	127.9(5)	112.6(3)
S1–Ru1–S2	170.5(1)	171.5(1)	170.3(1)	171.2(1)	173.9(1)
N1–Ru1–N2	81.4(2)	82.0(2)	80.1(2)	81.8(2)	83.2(1)
P1/S2A–Ru1–N3	90.6(2)	92.1(1)	89.2(2)	89.0(2)	93.5(1)
N1–Ru1–S1	82.6(1)	82.1(2)	82.2(2)	82.4(1)	84.4(1)
N1–Ru1–S2	88.5(2)	89.4(2)	88.4(2)	89.3(1)	100.7(1)
Ru1–N3–N3A/N4	173.5(2)	–	131.7(6)	130.1(3)	–

[a] **9**·1.5 CH_2Cl_2.

that P*i*Pr$_3$ has a stronger *trans* influence than N_2, N_2H_2, or NH_3. The N–N distance in the diazene ligands of **5** (127(1) pm) and **9** (127.9(5) pm) is nearly identical to that calculated for free N_2H_2 (124.7 pm).[16] This is typical for the 4c–6e$^-$ bonding system of the [M–NH=NH–M] chromophore of dinuclear diazene complexes.[17]

General properties and spectroscopic characterization of complexes 3–10: All isolated complexes have been characterized by standard spectroscopic methods and by elemental analysis. No accurate elemental analysis of [Ru(N_2)(P*i*Pr$_3$)('$N_2Me_2S_2$')] (**2**) could be obtained, since solid **2** always contains impurities of dinuclear complex **3**. The hydrazine complex [Ru(N_2H_4)(P*i*Pr$_3$)('$N_2Me_2S_2$')] (**6**) which proved stable only for a limited time in the presence of excessive hydrazine could be characterized only in solution by NMR spectroscopy. The dinuclear diazene complexes **5** and **9** exhibit a characteristic blue color that is due to their [Ru–NH=NH–Ru] chromophore.[17] As observed for the related [μ-N_2H_2{Ru(PPr$_3$)('S_4')}$_2$] and [μ-N_2H_2{Ru(PPh$_3$)('tpS_4')}$_2$] complexes,[18,19] two characteristic absorptions are found at $\lambda = 502$ nm ($\varepsilon = 14348$ L mol^{-1} cm^{-1}) and $\lambda = 650$ nm ($\varepsilon = 14493$ L mol^{-1} cm^{-1}).

All the other [Ru(L)(P*i*Pr$_3$)('$N_2Me_2S_2$')] complexes are yellow. The dinuclear N_2 and N_2H_2 complexes [μ-N_2{Ru(P*i*Pr$_3$)('$N_2Me_2S_2$')}$_2$] (**3**), [μ-N_2H_2{Ru(P*i*Pr$_3$)('$N_2Me_2S_2$')}$_2$] (**5**), and [{Ru(P*i*Pr$_3$)('$N_2Me_2S_2$')}-μ-N_2H_2{Ru(Cl)('$N_2Me_2S_2$-CH_2Cl')}] (**9**) exhibit moderate to low solubility in organic solvents, while all mononuclear [Ru(L)(P*i*Pr$_3$)('$N_2Me_2S_2$')] complexes are well soluble, for example, in benzene, toluene, or THF. CH_2Cl_2 is not suitable as a solvent because it slowly chloromethylates the complexes at the thiolate donors to give (S–CH_2Cl) complexes as described above. The dinuclear complex [{Ru($NCCH_3$)$_{0.8}$(NH_3)$_{0.2}$('$N_2Me_2S_2$')}$_2$] (**10**) is practically insoluble in all common solvents. Therefore, no solution spectra of complex **10** could be obtained.

The field-desorption (FD) mass spectra of all complexes exhibited the peak for the [Ru(P*i*Pr$_3$)('$N_2Me_2S_2$')] fragment at $m/z = 564$. The IR spectra in KBr featured the typical bands attributable to the [Ru(P*i*Pr$_3$)('$N_2Me_2S_2$')] fragment besides the specific bands for the co-ligands. Characteristic ν(N–H) absorptions were observed for the ammonia complex **4** (3350, 3306, 3240, and 3166 cm^{-1}) and for the dinuclear diazene complex **5** (3222 cm^{-1}). A strong ν(N≡N) band at 2047 cm^{-1} in solid state and at 2042 cm^{-1} in toluene solution is observed in the Raman spectra of the C_2-symmetric dinuclear dinitrogen complex **3**. The ^{13}C NMR spectra of the C_1-symmetric ammonia and hydrazine complexes **4** and **6** and of the C_2-symmetric dinuclear diazene complex **5** exhibit 12 signals for the aromatic C atoms and 4 signals for the aliphatic C atoms of the *N*-methyl groups and the ethylene bridge. Three additional signals are found for the P*i*Pr$_3$ co-ligands. The C_1-symmetric complex **9** exhibits 32 signals for the '$N_2Me_2S_2$' ligands, 3 signals for the P*i*Pr$_3$ co-ligand, and 1 signal for the (S-CH_2Cl) group. The ^{31}P{^{1}H,^{13}C} NMR spectra of **4**, **5**, and **6** always show one signal. The ^{1}H NMR spectra exhibit multiplets for the aromatic protons of **4**, **5**, **6**, and **9**, singlets for the *N*-methyl groups, a multiplet for the protons of the ethylene bridge, and multiplets for the P*i*Pr$_3$ co-ligands. Characteristic low-field-shifted singlets at $\delta = 13.61$ and 15.54 ppm are found for the NH protons in the dinuclear diazene complexes **5** and **9**. Doublets at $\delta = 4.41$ and 4.18 ppm and a singlet at $\delta = 3.58$ ppm are observed for the N_2H_4 ligand in **6**, whereas a singlet is observed at $\delta = 1.39$ ppm for the NH_3 ligand in the ammonia complex **4**.

Stereoisomers of the dinuclear N_2 complex 3: Due to the chirality of [Ru(P*i*Pr$_3$)('$N_2Me_2S_2$')] fragments, the dinuclear complex [μ-N_2{Ru(P*i*Pr$_3$)('$N_2Me_2S_2$')}$_2$] (**3**) can form three stereoisomers: (*R*,*R*)-**3**, (*S*,*S*)-**3**, and (*R*,*S*)-**3**. The *R*,*R* and *S*,*S* isomers could both be characterized by X-ray crystal structure determination. This gave rise to the question of whether the *R*,*S* diastereomer exists in either the solid state or in solution.

For this purpose, an X-ray powder diffractogram of solid **3** was recorded. The experimental diffractogram almost perfectly matched the one calculated for the molecular structures of (*R*,*R*)-**3** and (*S*,*S*)-**3**, thus confirming that the formation of solid [μ-N_2{Ru(P*i*Pr$_3$)('$N_2Me_2S_2$')}$_2$] (**3**) was exclusively limited to the *R*,*R* and *S*,*S* enantiomers.

Since (*R*,*R*)-**3** and (*S*,*S*)-**3** exhibit C_2 symmetry, the ^{31}P NMR spectrum should therefore display only one signal for both enantiomers. However, suspensions of sparingly soluble **3**, for example, in THF, afforded ^{31}P NMR spectra that exhibited three signals at $\delta = 42.06$, 40.23, and at 37.89 ppm (Figure 5).

An additional signal at $\delta = 46.09$ ppm was assigned to mononuclear **2**. At this point it must be mentioned that due to the weak solubility of the dinuclear N_2 complex, the main part of solid **3** remains undissolved.

The observation that the signals at $\delta = 42.06$, 40.23, and 37.89 ppm always occurred in a 1:1:1.7 ratio gave rise to the question of whether a dynamic behavior of **3** in THF solution had to be considered. In order to solve this problem, NMR studies and DFT calculations, with the BP86 density function[20] and the split-valence basis set of Ahlrichs and co-workers[21] (see the Supporting Information for additional information), were performed. The DFT calculations were carried out with simplified models for (*S*,*S*)- and (*R*,*S*)-**3**, where the phosphane has been replaced by PH_3 and PMe_3

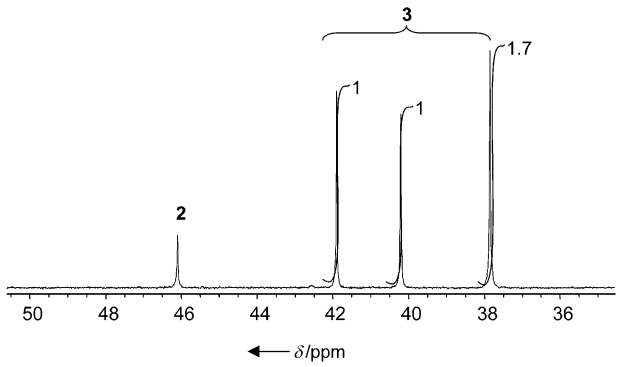

Figure 5. ^{31}P NMR spectrum of [μ-N_2[Ru(P*i*Pr$_3$)('$N_2Me_2S_2$')}$_2$] (**3**) in [D_8]THF.

model ligands. These calculations indicated that rotation of one [Ru(PMe$_3$)('$N_2Me_2S_2$')] fragment along the [Ru–N≡N–Ru] axis always results in two minimum structures for each diastereomer.

Since the rotation barriers calculated were lower than approximately 55 kJ mol^{-1}, thermal equilibria between these two minimum structures may be assumed. For both (*S*,*S*)- and (*R*,*S*)-[μ-N_2[Ru(PMe$_3$)('$N_2Me_2S_2$')}$_2$] minimum structures were found when the phosphane co-ligands adopted an orthogonal dihedral angle. With respect to these DFT calculations, the orthogonal arrangement of the phosphane ligands, as was found in the crystal structures of (*R*,*R*)- and (*S*,*S*)-**3**, may therefore be attributed to thermodynamic reasons.

In contrast to the *R*,*R* and *S*,*S* isomers of complex **3**, where the orthogonal order of the phosphane co-ligands results in C_2 symmetry, the hypothetical diastereomer (*R*,*S*)-[μ-N_2[Ru(P*i*Pr$_3$)('$N_2Me_2S_2$')}$_2$] ((*R*,*S*)-**3**) is expected to exhibit C_1 symmetry if the phosphane co-ligands adopt an orthogonal dihedral angle of 90°. As a consequence, the P*i*Pr$_3$ substituents in (*R*,*S*)-**3** become magnetically inequivalent.

These findings therefore supported the speculation that two of the three observed ^{31}P NMR signals have to be assigned to the formation of the C_1-symmetric diastereomer (*R*,*S*)-[μ-N_2[Ru(P*i*Pr$_3$)('$N_2Me_2S_2$')}$_2$] ((*R*,*S*)-**3**).

^{31}P-EXSY spectra finally confirmed that the formation of (*R*,*S*)-[μ-N_2[Ru(P*i*Pr$_3$)('$N_2Me_2S_2$')}$_2$] ((*R*,*S*)-**3**) occurred due to a dynamic process in solution. Upon dissolution, dinuclear (*R*,*R*)- and (*S*,*S*)-**3** dissociate, forming racemic mononuclear **2** and the coordinatively unsaturated [Ru(P*i*Pr$_3$)('$N_2Me_2S_2$')] fragment, which is highly reactive and cannot be detected. Upon reaction with traces of N_2, it can form mononuclear **2**. Recombination of [Ru(P*i*Pr$_3$)('$N_2Me_2S_2$')] fragments with mononuclear (*R*)- or (*S*)-**2** leads to the formation of dinuclear (*R*,*R*)- and (*S*,*S*)-**3**, which give rise to one singlet, and to (*R*,*S*)-**3** which gives rise to two further signals in a 1:1 ratio.

Experiments to reduce the mono- and dinuclear N_2 complexes 2 and 3: The isolation of the N_2 complexes **2** and **3** prompted experiments to reduce them to the corresponding N_2H_2, N_2H_4, and NH_3 compounds. Since the unstable N_2H_2 molecule could be stabilized by steric shielding and the formation of strong S···H···S bridges within dinuclear N_2H_2 complexes of the type [S_nM–N_2H_2–MS_n], where S_nM denotes a metal sulfur complex fragment,[22] the dinuclear N_2 complex [μ-N_2[Ru(P*i*Pr$_3$)('$N_2Me_2S_2$')}$_2$] (**3**) seemed to be a favorable candidate for reduction experiments. However, the high tendency of **3** to form the mononuclear N_2 complex **2** and the coordinatively unsaturated [Ru(P*i*Pr$_3$)('$N_2Me_2S_2$')] fragment in solution represented a serious obstacle with respect to the reduction of the N_2 ligand in **3**. But even with the mononuclear N_2 complex **2**, no reduction of the N_2 ligand could be achieved. Until now, all attempts to reduce the N_2 ligand by using common reducing reagents like Zn, $CoCp_2$, or H_2 and subsequent protonation with HBF_4, H_2O, or ammonium salts as the proton sources have failed.

Conclusions

This paper describes the first series of complexes where N_2, N_2H_2, N_2H_4, and NH_3 bind to an identical transition-metal sulfur complex fragment under ambient conditions. Although biological N_2 fixation takes place at the FeMo sites of the FeMo cofactor, the ruthenium complexes **2**–**7** are of relevance for determining the mechanism of this important reaction. Unfortunately, the original idea that the dinuclear nitrogen complex **3** may be reduced to the corresponding diazene complex **5** could not be verified. This failure may arise from the fact that **3** undergoes an efficient dissociation into the mononuclear N_2 complex **2** in solution. Although efforts to reduce **2** have not yet been successful, the high electron density at the metal center of the [Ru(P*i*Pr$_3$)('$N_2Me_2S_2$')] fragment is most likely responsible for the smooth reaction with hydrazine. In this reaction, the first step is the formation of the hydrazine complex **6** that disproportionates to give the corresponding diazene complex **7** and the ammonia complex **4**. Since the ammonia ligand in **4** is easily replaced by N_2, a catalytic cycle becomes feasible (Figure 6).

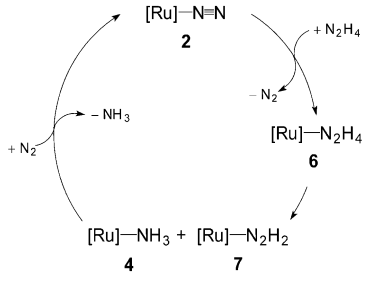

Figure 6. Overview of the reactions reported. [Ru] = [Ru(P*i*Pr$_3$)('$N_2Me_2S_2$')].

The mononuclear diazene complex **7** could not be isolated because of its high tendency to form the bridged complex **5**. The driving force of this reaction may be rationalized as the stabilization of the unstable N_2H_2 molecule by steric shielding of the NH protons through strong S···H···S bridges within the metal sulfur complex fragments.[22]

Having these complexes in hand, we are hopeful that the N_2 complex **2** or a more stable derivative of the dinuclear N_2 complex **3** can be transformed by coupled [$2H^+/2e^-$] reduction steps into the corresponding N_2H_2, N_2H_4, and NH_3 complexes. With this goal in mind, further investigations will be carried out to find the appropriate conditions.

Experimental Section

General: Unless noted otherwise, all reactions and spectroscopic measurements were carried out at room temperature under argon or nitrogen by using standard Schlenk techniques in absolute solvents derived from Fluka or Acros Chemicals. As far as possible, all reactions were monitored by IR and NMR spectroscopy. IR spectra in solution were recorded in CaF_2 cuvettes with compensation of the solvent bands, solids were measured as KBr pellets. NMR spectra were recorded, unless otherwise specified, at room temperature (20 °C) in the solvents indicated. Chemical shifts are given in ppm and reported relative to residual protonated solvent resonances (^1H, ^{13}C) or external standards: $BF_3{\cdot}Et_2O$ (^{11}B), H_3PO_4 (^{31}P). EXSY spectra were measured by the phase-sensitive NOESY method. Mass spectra were measured in the field-desorption (FD) mode. Solid-state X-ray powder diffractograms were measured in a 5 mm Mark tube. The physical measurements were carried out with the following instruments: IR spectroscopy: Perkin–Elmer 983, Perkin–Elmer 1600 FTIR, and Perkin–Elmer 16PC FTIR; NMR spectroscopy: JEOL FT-JNM-GX 270, Lambda LA 400, JEOL Alpha 500; mass spectrometry: Jeol MSTATION 700; UV/Vis/NIR spectroscopy: Shimadzu UV-3101 PC; Raman spectroscopy: Bruker FT-Raman RFS100/S; X-ray powder diffractometry: Guinier diffractometer, type Huber 601 with counting tube.

[Ru(NCCH$_3$)(P*i*Pr$_3$)('$N_2Me_2S_2$')][5] (**1**), [Ru(N_2)(P*i*Pr$_3$)('$N_2Me_2S_2$')][5] (**2**), [μ-N_2{Ru(P*i*Pr$_3$)('$N_2Me_2S_2$')}$_2$][6] (**3**), and $K_2N_2(CO_2)_2$[23] were prepared as described in the literature. Anhydrous N_2H_4 was obtained by double distillation of $N_2H_4{\cdot}H_2O$ over KOH. Caution: Anhydrous N_2H_4 is an explosive substance and should always be handled behind a protection shield!

Improved synthesis of [Ru(N_2)(P*i*Pr$_3$)('$N_2Me_2S_2$')] (2): An intense stream of N_2 was passed through a solution of **4** (850 mg, 1.46 mmol) in toluene (200 mL) at 55 °C for 2 h. The solvent was replaced every 20 min. The reaction was terminated when IR monitoring of the reaction showed no further increase of the ν(N≡N) band of **2**. The yellow reaction solution was filtered and reduced in volume to 1 mL by a stream of nitrogen. Addition of *n*-pentane (30 mL) yielded a yellow solid, which was separated after 1 h, washed with *n*-pentane (15 mL), and dried in a stream of nitrogen for 2 h. Yield: 760 mg (88 %); ^1H NMR (399.65 MHz, [D$_8$]THF): δ = 7.48 (d, ^3J(H,H) = 8.2 Hz, 1H, C$_6$**H**$_4$), 7.40 (d, ^3J(H,H) = 8.0 Hz, 1H, C$_6$**H**$_4$), 7.37 (d, ^3J(H,H) = 7.2 Hz, 1H, C$_6$**H**$_4$), 7.23 (d, ^3J(H,H) = 8.2 Hz, 1H, C$_6$**H**$_4$), 6.91–6.75 (m, 4H, C$_6$**H**$_4$), 3.42 (s, 3H, C**H**$_3$), 3.38 (s, 3H, C**H**$_3$), 3.30–2.40 (m, 4H, C$_2$**H**$_4$), 2.30–2.23 (m, 3H, P[C**H**(CH$_3$)$_2$]$_3$), 1.37–1.30 ppm (m, 18H, P[C**H**(CH$_3$)$_2$]$_3$); $^{13}C\{^1H\}$ NMR (100.40 MHz, [D$_8$]toluene): δ = 152.2, 151.8, 150.5, 150.0, 131.2, 131.1, 126.0, 125.7, 120.7, 120.5, 120.1, 119.2 (**C**$_6$H$_4$), 67.1, 60.8 (**C**H$_3$), 50.8, 46.9 (**C**$_2$H$_4$), 27.1 (d, ^1J(P,C) = 18 Hz, P[**C**H(CH$_3$)$_2$]$_3$), 21.8, 20.5 ppm (P[CH(**C**H$_3$)$_2$]$_3$); $^{31}P\{^1H\}$ NMR (161.70 MHz, [D$_8$]THF): δ = 46.07 ppm (**P**[C$_3$H$_7$]$_3$); IR (KBr): $\tilde{\nu}$ = 2113 cm^{-1} (N≡N); MS (^{102}Ru, toluene): *m*/*z* = 564 [M^+-N_2]$^+$; elemental analysis: calcd (%) for $C_{25}H_{39}N_4S_2RuP$ (591.83): C 50.73, H 6.66, N 9.46, S 10.83; found: C 51.68, H 7.40, N 6.95, S 10.77.

[Ru(NH_3)(P*i*Pr$_3$)('$N_2Me_2S_2$')] (4): NH_3 was passed through a solution of **1** (1.06 g, 1.67 mmol) in THF (60 mL) at 50 °C for 1 h. The solvent was replaced every 10 min. The reaction was terminated when IR monitoring of the reaction no showed longer the ν(CN) band of **1**. The yellow reaction solution was filtered and reduced to 2 mL in volume. Addition of MeOH (30 mL) yielded a yellow solid, which was separated after 1 h, washed with MeOH (10 mL) and *n*-pentane (15 mL), and dried in vacuo. Yield: 850 mg (87 %); ^1H NMR (399.65 MHz, [D$_8$]THF): δ = 7.53 (d, ^3J(H,H) = 7.6 Hz, 1H, C$_6$**H**$_4$), 7.42 (d, ^3J(H,H) = 7.8 Hz, 1H, C$_6$**H**$_4$), 7.32 (d, ^3J(H,H) = 8.2 Hz, 1H, C$_6$**H**$_4$), 7.06 (d, ^3J(H,H) = 8.4 Hz, 1H, C$_6$**H**$_4$), 6.81–6.60 (m, 4H, C$_6$**H**$_4$), 3.27 (s, 3H, C**H**$_3$), 3.27 (s, 3H, C**H**$_3$), 2.89–2.19 (m, 4H, C$_2$**H**$_4$), 2.10–2.04 (m, 3H, P[C**H**(CH$_3$)$_2$]$_3$), 1.39 (s, 3H, N**H**$_3$), 1.40–1.10 ppm (m, 18H, P[CH(C**H**$_3$)$_2$]$_3$); $^{13}C\{^1H\}$ NMR (100.40 MHz, [D$_8$]THF): δ = 156.3, 156.2, 154.6, 152.0, 132.6, 132.1, 125.7, 125.4, 122.2, 120.1, 119.8, 119.6 (**C**$_6$H$_4$), 69.3, 62.8 (**C**H$_3$), 54.4, 46.6 (**C**$_2$H$_4$), 28.4 (d, ^1J(P,C) = 16.5 Hz, P[**C**H(CH$_3$)$_2$]$_3$), 21.1, 19.7 ppm (P[CH(**C**H$_3$)$_2$]$_3$); $^{31}P\{^1H\}$ NMR (161.70 MHz, [D$_8$]THF): δ = 56.94 ppm (**P**[C$_3$H$_7$]$_3$); IR (KBr): $\tilde{\nu}$ = 3350, 3306, 3240, 3166 cm^{-1} (N–H); MS (^{102}Ru, THF): *m*/*z* = 564 [M^+-NH_3]$^+$; elemental analysis: calcd (%) for $C_{25}H_{42}N_3S_2RuP$ (580.85): C 51.70, H 7.29, N 7.23, S 11.04; found: C 51.50, H 7.55, N 7.23, S 11.35.

[μ-N_2H_2{Ru(P*i*Pr$_3$)('$N_2Me_2S_2$')}$_2$] (5): Method A with N_2H_4: N_2H_4 (1 N solution in THF, 5 mL, 5 mmol) was added to solid **1** (360 mg, 0.6 mmol). Within 6 h the color of the solution changed from yellow to orange-red and finally to deep blue. The solution was filtered and MeOH (40 mL) was added dropwise. Within 12 h, grey-blue microcrystals were formed, which were separated, washed with MeOH (27 mL) and Et_2O (10 mL), and dried in vacuo. Yield: 250 mg (68 %); ^1H NMR (399.65 MHz, [D$_8$]THF): δ = 13.61 (s, 2H, N_2**H**$_2$), 7.56 (d, ^3J(H,H) = 7.9 Hz, 2H, C$_6$**H**$_4$), 7.38 (d, ^3J(H,H) = 8.2 Hz, 2H, C$_6$**H**$_4$), 7.35 (d, ^3J(H,H) = 8.2 Hz, 2H, C$_6$**H**$_4$), 7.06 (d, ^3J(H,H) = 8.2 Hz, 2H, C$_6$**H**$_4$), 6.99–6.66 (m, 8H, C$_6$**H**$_4$), 3.16 (s, 6H, C**H**$_3$), 3.08 (s, 6H, C**H**$_3$), 3.25–2.23 (m, 8H, C$_2$**H**$_4$), 2.07–1.89 (m, 6H, P[C**H**(CH$_3$)$_2$]$_3$), 1.34–0.89 ppm (m, 36H, P[CH(C**H**$_3$)$_2$]$_3$); $^{13}C\{^1H\}$ NMR (100.40 MHz, [D$_8$]THF): δ = 159.5, 159.0, 157.3, 154.4, 136.6, 136.3, 131.6, 130.0, 127.2, 126.7, 125.1, 123.6 (**C**$_6$H$_4$), 73.1, 67.2 (**C**$_2$H$_4$), 57.5, 50.5 (**C**H$_3$), 26.3 (d, ^1J(P,C) = 18 Hz, P[**C**H(CH$_3$)$_2$]$_3$), 25.0, 24.9 ppm (P[CH(**C**H$_3$)$_2$]$_3$); $^{31}P\{^1H\}$ NMR (161.70 MHz, [D$_8$]THF): δ = 40.62 ppm (**P**[C$_3$H$_7$]$_3$); IR (KBr): $\tilde{\nu}$ = 3222 cm^{-1} (N–H); UV/Vis (THF): λ_{max} (ε) = 325 (39856), 502 (14348), 650 nm (14493 L mol^{-1} cm^{-1}); MS (^{102}Ru, toluene): *m*/*z* = 564 [Ru(P*i*Pr$_3$)('$N_2Me_2S_2$')]$^+$; elemental analysis: calcd (%) for $C_{50}H_{80}N_6P_2Ru_2S_4$ (1157.52): C 51.48, H 7.11, N 7.06, S 10.78; found: C 51.88, H 6.97, N 7.26, S 11.11.

[μ-N_2H_2{Ru(P*i*Pr$_3$)('$N_2Me_2S_2$')}$_2$] (5): Method B with $K_2N_2(CO_2)_2$ and acetic acid: Acetic acid (12.5 mL, 2.5 mmol, 0.2 M in H_2O) was added to a yellow suspension of $K_2N_2(CO_2)_2$ (498 mg, 2.7 mmol) and **1** (310 mg, 0.49 mmol) in THF (20 mL). Upon gas evolution the solution changed color to deep blue within 1.5 h and grey-blue microcrystals precipitated. The aqueous layer was removed and the crystallization was driven to completeness by adding MeOH (70 mL) dropwise to the THF layer. After 12 h, the grey-blue microcrystals were separated, washed with MeOH (15 mL) and Et_2O (6 mL), and dried in vacuo. Yield: 130 mg (46 %).

[Ru(N_2H_4)(P*i*Pr$_3$)('$N_2Me_2S_2$')] (6): Anhydrous N_2H_4 (8 μL, 0.28 mmol) was injected into a 5 mm NMR tube containing a yellow-green solution of **1** (25 mg, 0.042 mmol) in [D$_8$]THF (0.8 mL). Upon gas evolution, a deep yellow solution of **6** formed; this was immediately characterized by NMR spectroscopy. ^1H NMR (399.65 MHz, [D$_8$]THF): δ = 7.54 (d, ^3J(H,H) = 7.6 Hz, 1H, C$_6$**H**$_4$), 7.42 (d, ^3J(H,H) = 7.6 Hz, 1H, C$_6$**H**$_4$), 7.38 (d, ^3J(H,H) = 8.2 Hz, 1H, C$_6$**H**$_4$), 7.06 (d, ^3J(H,H) = 8.2 Hz, 1H, C$_6$**H**$_4$), 6.82–6.61 (m, 4H, C$_6$**H**$_4$), 4.41 (d, ^2J(H,H) = 10.8 Hz, 1H, RuN**H**$_2$NH$_2$), 4.18 (d, ^2J(H,H) = 10.8 Hz, 1H, RuN**H**$_2$NH$_2$), 3.58 (s, 2H, RuNH$_2$N**H**$_2$), 3.45 (s, 3H, C**H**$_3$), 3.24 (s, 3H, C**H**$_3$), 3.28–2.30 (m, 4H, C$_2$**H**$_4$), 2.20–2.12 (m, 3H, P[C**H**(CH$_3$)$_2$]$_3$), 1.41–1.25 ppm (m, 18H, P[CH(C**H**$_3$)$_2$]$_3$); $^{13}C\{^1H\}$ NMR (100.40 MHz, [D$_8$]THF): δ = 155.5, 155.1, 155.0, 152.5, 132.3, 132.0, 125.8, 125.5, 122.3, 120.5, 120.2, 120.1, 119.4 (**C**$_6$H$_4$), 69.3, 63.0 (**C**H$_3$), 54.0, 47.0 (**C**$_2$H$_4$), 28.7 (d, ^1J(P,C) = 21 Hz, P[**C**H(CH$_3$)$_2$]$_3$), 21.2, 20.0 ppm (P[CH(**C**H$_3$)$_2$]$_3$); $^{31}P\{^1H\}$ NMR (161.70 MHz, [D$_8$]THF): δ = 53.07 ppm (**P**[C$_3$H$_7$]$_3$).

[{Ru(P*i*Pr$_3$)('$N_2Me_2S_2$')}-μ-N_2H_2{Ru(Cl)('$N_2Me_2S_2CH_2Cl$')}] (9): A blue solution of **5** (250 mg, 0.21 mmol) in CH_2Cl_2 (25 mL) was stirred for three days. A violet solution formed, which was filtered over Al_2O_3 (Act. II). The Al_2O_3 was washed with CH_2Cl_2 (40 mL) and the filtrate was evaporated to dryness. The residue was dissolved in CH_2Cl_2 (20 mL) and *n*-hexane (40 mL) was added. Reduction of the solution by volume to 20 mL yielded a violet solid, which was separated, washed with *n*-hexane (10 mL), and dried in vacuo. Yield: 110 mg (50 %); ^1H NMR (269.7 MHz, CD_2Cl_2): δ = 15.40 (s, 2H, N_2**H**$_2$), 8.25–6.65 (m, 16H, C$_6$**H**$_4$), 5.16–4.95 (m, 2H, C**H**$_2$Cl), 3.49 (s, 3H, C**H**$_3$), 3.28 (s, 3H, C**H**$_3$), 3.93–1.94 (m, 8H, C$_2$**H**$_4$), 2.35–2.05 (m, 3H, P[C**H**(CH$_3$)$_2$]$_3$), 2.22 (s, 3H, C**H**$_3$), 2.12 (s, 3H, C**H**$_3$), 1.50–1.00 ppm (m, 18H, P[CH(C**H**$_3$)$_2$]$_3$); $^{13}C\{^1H\}$ NMR (100.4 MHz, CD_2Cl_2): δ = 154.8, 153.4, 153.1, 153.0, 152.9, 151.9, 150.3, 134.7, 132.6, 131.9, 131.8, 131.7, 131.1, 128.8, 127.1, 126.6, 126.2, 124.0, 123.2, 122.9, 121.4, 120.8, 120.4, 120.1 (**C**$_6$H$_4$), 68.0, 67.1, 65.0, 62.6 (**C**$_2$H$_4$), 56.6 (**C**H$_2$), 54.4, 52.4, 51.8, 46.2 (**C**H$_3$), 28.0 (P[**C**H(CH$_3$)$_2$]$_3$), 21.4 ppm

($P[CH(CH_3)_2]_3$); $^{31}P\{^1H\}$ NMR (161.7 MHz, CD_2Cl_2): $\delta = 43.00$ ppm ($P[C_3H_7]_3$); IR (KBr): $\tilde{\nu} = 3188\ cm^{-1}$ (N–H); MS (^{102}Ru, CH_2Cl_2): $m/z = 564$ $[Ru(PiPr_3)(`N_2Me_2S_2')]^+$; elemental analysis: calcd (%) for $C_{42.33}H_{61.66}Cl_{2.66}N_6PRu_2S_4$ (1110.30): C 45.76, H 5.60, N 7.57, S 11.55; found: C 45.79, H 5.99, N 7.28, S 11.12.

$[\{Ru(NCCH_3)_{0.8}(NH_3)_{0.2}(`N_2Me_2S_2')\}_2]$ (10): N_2H_4 (1 N solution in THF, 5 mL, 5 mmol) was added to solid **1** (360 mg, 0.6 mmol). Within 6 h the color of the solution changed from yellow to orange-red and finally to deep blue. The solution was filtered and MeOH (40 mL) was added dropwise. Within 12 h, grey-blue microcrystals of complex **5** formed, which were removed. Within eight weeks, orange-brown microcrystals precipitated from the mother liquor. They were removed and dried in vacuo without any further washing. Yield: 40 mg (13 %); IR (KBr): $\tilde{\nu} = 2238\ cm^{-1}$ (N≡C); MS (^{102}Ru, toluene): $m/z = 807$ $[\{Ru(`N_2Me_2S_2')\}_2]^+$; elemental analysis: calcd (%) for $C_{37.6}H_{51.6}N_6O_{2.4}Ru_2S_4$ (956.43): C 47.22, H 5.44, N 8.88, S 13.41; found: C 46.96, H 5.48, N 8.96, S 13.57.

X-ray crystal structure analysis of 3, 4, 5, 9·1.5 CH_2Cl_2, and 10: Yellow-green blocks of **3** were formed upon layering a saturated toluene solution of **3** with *n*-pentane at 20 °C. Yellow prisms of **4** were grown by slow cooling of a hot saturated THF/MeOH solution of **4** to room temperature. Black blocks of **5** were obtained within five weeks upon layering a saturated THF solution of **5** with MeOH at −34 °C. Black plates of **9**·1.5 CH_2Cl_2 were grown within four weeks upon layering a CH_2Cl_2/THF solution of **9** with acetone at −30 °C. Brown blocks of **10** precipitated within two months from filtered THF/MeOH mother liquors from the reaction of **1** with N_2H_4. Suitable single crystals were coated with inert perfluoropolyalkyl ether. The data for **3**, **4**, and **9** were collected on a Siemens P4 diffractometer and those for **5** and **10** on a Nonius Kappa CCD diffractometer. The radiation used was $Mo_{K\alpha}$ with $\lambda = 71.073$ pm, and the scan technique was ω scans in each case. Data were corrected for Lorentz and polarization effects. Absorption effects were corrected by using either Psi scans[24] (**3**, **4**, **9**·1.5 CH_2Cl_2) or multiscans from symmetry equivalents (**5**: SORTAV,[25] **10**: SABABS[26]). The structures were solved by direct methods and refined by using full-matrix least-squares procedures on F^2 (SHELXTL NT 5.10). All non-hydrogen atoms were refined anisotropically. Treatment of hydrogen atoms: Hydrogen atoms for **3**, **5**, and **10** are geometrically positioned and allowed to ride on their carrier atoms. Their isotropic displacement parameters have been tied to the corresponding $U_{eq.}$ parameters of their carrier atoms by a factor of 1.2 or 1.5. Hydrogen atoms for **4** and **9** have been derived from a difference Fourier synthesis. Their positional parameters and a common isotropic displacement parameter have been kept fixed during the refinement. The unit cell of **9** contains a total of three CH_2Cl_2 solvate molecules, two of which are disordered. No hydrogen atoms have been included for the solvate molecules. The unit cell of **10** contains a total of 2.4 molecules of MeOH per formula unit. The fractional amount of 0.4 MeOH is due to the fact that a MeOH is present when NH_3 is the co-ligand, while no MeOH can be found when CH_3CN acts as co-ligand. Table 2 lists selected crystallographical data for compounds **3**, **4**, **5**, **9**·1.5 CH_2Cl_2, and **10**.

CCDC-188834 and 188835 (**3**; two crystals of different polarity), CCDC-223492 (**4**), CCDC-223493 (**5**), CCDC-223494 (**9**), and CCDC-223495 (**10**) contain the supplementary crystallographic data for this paper. These data can be obtained free of charge via www.ccdc.cam.ac.uk/conts/retrieving.html (or from the Cambridge Crystallographic Data Centre, 12 Union Road, Cambridge CB2 1EZ, UK; fax: (+44) 1223-336-033; or deposit@ccdc.cam.uk).

X-ray powder diffractometry: A sample of solid $[\mu\text{-}N_2\{Ru(PiPr_3)(`N_2Me_2S_2')\}_2]$ (**3**) was filled into a 5 mm Mark tube and measured on a Guinier diffractometer, type Huber 601 with counting tube. The Mark tube was rotated during the measurement. The diffractogram was then compared to an X-ray powder diffractogram that was calculated on the basis of the X-ray crystal structure data of (*R*,*R*)-**3**. The measured powder diffractogram of **3** was found to correspond to the calculated one. Solid $[\mu\text{-}N_2\{Ru(PiPr_3)(`N_2Me_2S_2')\}_2]$ (**3**) consists of more than 98 % of (*R*,*R*)- and (*S*,*S*)-**3**.

The powder diffractogram showed additional peaks of very low intensity (below 2 %) which indicated a second crystalline solid. These peaks could be caused by a second polymorph form of (*R*,*R*)-**3** or by a further crystalline substance. It was impossible to define these additional peaks as a second isomer of (*R*,*R*)- or (*S*,*S*)-**3** because the (hypothetical or actual) crystal structure of this second isomer is unknown, and the additional reflexes are too low in intensity for a calculation of the crystal structure of this component with respect to the powder diffractogram. The sample of solid **3** did not contain the mononuclear complex **2**. All percentages referred to crystalline substances. Amorphous substances cannot be detected by X-ray powder diffractometry.

Table 2. Selected crystallographic data for **3**, **4**, **5**, **9**·1.5 CH_2Cl_2, and **10**·2.4 MeOH.

	3	**4**	**5**	**9**·1.5 CH_2Cl_2	**10**·2.4 MeOH
formula	$C_{50}H_{78}N_6P_2Ru_2S_4$	$C_{25}H_{42}N_3PRuS_2$	$C_{50}H_{80}N_6P_2Ru_2S_4$	$C_{43.5}H_{64}Cl_5N_6PRu_2S_4$	$C_{37.6}H_{51.6}N_6O_{2.4}Ru_2S_4$
M_r	1155.50	580.78	1157.52	1209.61	956.43
crystal size [mm]	0.60 × 0.26 × 0.18	0.34 × 0.24 × 0.16	0.34 × 0.07 × 0.07	0.60 × 0.50 × 0.20	0.37 × 0.28 × 0.09
$F(000)$	4816	608	4832	2476	981
crystal system	orthorhombic	triclinic	orthorhombic	triclinic	monoclinic
space group	*Fdd*2	$P\bar{1}$	*Fdd*2	$P\bar{1}$	$P2_1/c$
a [pm]	2943.3(3)	1034.8(1)	2959.8(2)	1527.2(1)	1324.3(2)
b [pm]	3662.8(4)	1161.4(1)	3662.3(4)	1585.5(2)	1099.1(3)
c [pm]	960.6(2)	1233.2(1)	956.9(1)	2249.5(2)	1362.1(2)
α [°]	90.0	69.385(7)	90.0	80.87(1)	90.0
β [°]	90.0	77.708(8)	90.0	74.28(1)	94.0(7)
γ [°]	90.0	76.617(9)	90.0	88.66(1)	90.0
V [nm^3]	10.356(3)	1.3354(2)	10.372(2)	5.1756(9)	1.9777(4)
Z	8	2	8	4	2
ρ_{calcd} [g cm^{-3}]	1.482	1.444	1.482	1.552	1.606
μ [mm^{-1}]	0.847	0.822	0.846	1.072	1.018
T [K]	200	210	100	200	100
2θ range [°]	3.5–56.0	3.5–54.0	6.8–52.0	3.7–54.0	6.5–56.6
T_{min}/T_{max}	0.417/0.456	0.727/0.845	0.702/0.996	0.272/0.334	0.820/1.000
measured reflections	6625	6647	21 238	25 130	38 260
independent reflections	6256	5675	5065	22 521	4891
R_{int}	0.0325	0.0461	0.0954	0.0295	0.0527
observed reflections[a]	5057	3981	4270	15 782	4018
R_1[a]/wR_2	0.0433/0.0881	0.0501/0.1319	0.0521/0.1234	0.0492/0.1214	0.0275/0.0563
refinement parameters	297	289	297	1162	261
$\Delta\delta_{max/min}$	0.580/−0.463	0.687/−0.687	1.116/−0.566	1.091/−0.878	0.465/−0.633
absolute structure parameters	−0.03(4)	–	0.00(5)	–	–

[a] $F_o \geq 4.0\sigma(F)$.

EXSY spectra: EXSY spectra were measured on a JEOL Alpha 500 apparatus by the phase-sensitive NOESY method ($90°-\tau_1-\tau_{mix}-90°-$FID, $\tau_{mix}=1000$ ms; $90°-$pulse, 12.5 ms, spectral width = 3400 Hz; 256 data points in f_2; 64 data points in f_1, zero-filled to 128 data points; relaxation delay = 2.0 s.

DFT calculations: For all calculations, the density functional programs provided by the TURBOMOLE 5.1 suite were used.[27] All results are obtained from Kohn–Sham calculations by using effective core potentials for Ru from the Stuttgart–Cologne groups as implemented in TURBOMOLE. We employ the Becke–Perdew functional dubbed BP86.[20] In combination with the BP86 functional we use the resolution of the identity (RI) technique.[28,29] The split-valence basis set of Ahlrichs and coworkers,[21] which features polarization functions on all atoms except hydrogen atoms, was employed. Structure optimizations of the *R*,*S* and *S*,*S* isomer models of **3** were carried out. In these calculations, the phosphanes were modelled by PH_3 (carried out in C_i symmetry) and by PMe_3 (carried out in C_1 symmetry). Consequently, the rotational energy curve of the *S*,*S* model system with PMe_3 as the phosphane ligand shows two minima separated by two potential energy wells of different magnitude. This different magnitude is a result of the steric repulsions of the methyl groups at the nitrogen atoms (of the chelate ligands) and of the hydrogen atoms of the phosphane ligands. While we observe a weak repulsion if the methyl group interacts with the phosphane, the repulsion is larger in the case of the conformation, which shows phosphane–phosphane and methyl–methyl interactions.

Figure 7 shows the rotational energy curve of a rotation about the Ru−N≡N−Ru axis in (*S*,*S*)-[μ-N_2{Ru(PMe_3)('$N_2Me_2S_2$')}$_2$], which produces two stable conformers with two phosphanes in orthogonal positions. These conformers are separated by barriers of approximately 55 kJ mol^{-1}, which result from a steric hindrance of the phosphanes and the methyl groups of the amine nitrogen atoms in the chelate ligand. The steric hindrance is small if two phosphane–methyl-group repulsions occur, when compared with the phosphane–phosphane and methyl–methyl repulsions in the maximum-rotation-energy structure. Particularly for this maximum-energy structure, a finer rotational structure was found around the maximum, which can induce local maxima and minima owing to the hindered rotation of the phosphane's methyl groups.

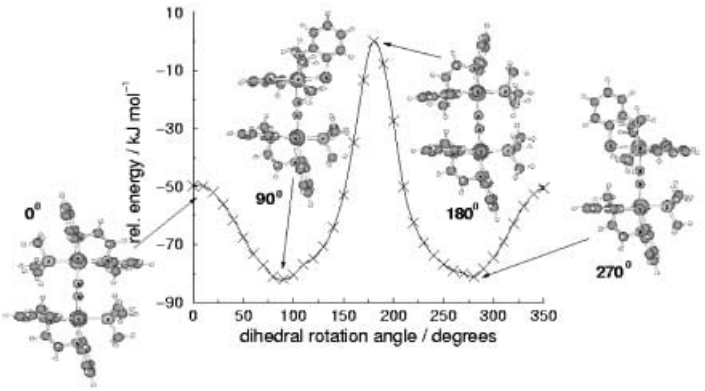

Figure 7. Curve of rotation about the Ru−N≡N−Ru axis, which produces two stable conformers in which the two phosphanes are in orthogonal positions.

Acknowledgement

Help from Prof. Dr. H. Kisch for supporting assistance, from Dr. R. Herrmann, Institut für Chemie- und Bioingenieurwesen, Universität Erlangen-Nürnberg, and from Prof. Dr. M. U. Schmidt, Institut für Anorganische Chemie, Universität Frankfurt/Main, for the measurement of X-ray powder diffractograms is gratefully acknowledged. We thank the Deutsche Forschungsgemeinschaft (SFB 583) and the Fonds der Chemischen Industrie for financial support.

[1] a) J. Kim, D. C. Rees, *Science* **2002**, *297*, 1696–1998; b) M. M. Georgiadis, H. Komiya, P. Chakrabarti, D. Woo, J. J. Kornuc, D. C. Rees, *Science* **1992**, *257*, 1653–1659; c) J. Kim, D. C. Rees, *Science* **1992**, *257*, 1677–1682; d) J. Kim, D. C. Rees, *Nature* **1992**, *360*, 553–560; e) J. Kim, D. Woo, D. C. Rees, *Biochemistry* **1993**, *32*, 7104–7105; f) M. K. Chan, J. Kim, D. C. Rees, *Science* **1993**, *260*, 792–794; g) J. T. Bolin, N. Campobasso, S. W. Muchmore, T. V. Morgan, L. E. Mortensen in *Molybdenum Enzymes, Cofactors and Model Systems* (Eds.: E. I. Stiefel, D. Coucouvanis, W. E. Newton), American Chemical Society, Washington DC, 1993, 186–195.

[2] a) R. Hoffmann, H. Deng, *Angew. Chem.* **1993**, *105*, 1125–1128; *Angew. Chem. Int. Ed. Engl.* **1993**, *32*, 1062–1065; b) I. G. Dance, *J. Biol. Inorg. Chem.* **1996**, *1*, 581–586; c) K. K. Stavrev, M. C. Zerner, *Chem. Eur. J.* **1996**, *2*, 83–87; d) P. E. M. Siegbahn, M. R. A. Blomberg, *Chem. Rev.* **2000**, *100*, 421–437; e) Y. Chen, M. Hartmann, G. Frenking, *Eur. J. Inorg. Chem.* **2001**, 1441–1448; f) D. Sellmann, J. Sutter, *J. Biol. Inorg. Chem.* **1996**, *1*, 587–593; g) D. Sellmann, A. Fürsattel, J. Sutter, *Coord. Chem. Rev.* **2000**, *200*, 541–561; h) H. I. Lee, B. J. Hales, B. M. Hoffman, *J. Am. Chem. Soc.* **1997**, *119*, 10121–10126.

[3] a) R. R. Eady, G. J. Leigh, *J. Chem. Soc. Dalton Trans.* **1994**, 2739–2744; b) M. D. Fryzuk, S. A. Johnson, *Coord. Chem. Rev.* **2000**, *200*, 379–409; c) M. Hidai, Y. Mizobe, *Chem. Rev.* **1995**, *95*, 1115–1133; d) J. B. Howard, D. C. Rees, *Chem. Rev.* **1996**, *96*, 2965–2982.

[4] B. K. Burgess, D. J. Low, *Chem. Rev.* **1996**, *96*, 2983–3011.

[5] D. Sellmann, B. Hautsch, A. Rösler, F. W. Heinemann, *Angew. Chem.* **2001**, *113*, 1553–1558; *Angew. Chem. Int. Ed.* **2001**, *40*, 1505–1507.

[6] D. Sellmann, A. Hille, F. W. Heinemann, M. Moll, A. Rösler, J. Sutter, G. Brehm, M. Reiher, B. A. Hess, S. Schneider, *Inorg. Chim. Acta* **2003**, *348*, 194–198.

[7] D. Sellmann, A. Brandl, R. Endell, *J. Organomet. Chem.* **1975**, *97*, 229–243, and references therein.

[8] D. Sellmann, A. Brandl, R. Endell, *Z. Naturforsch. B* **1978**, *33*, 542–553.

[9] D. Sellmann, A. Hennige, *Angew. Chem.* **1997**, *109*, 270–271; *Angew. Chem. Int. Ed. Engl.* **1997**, *36*, 276–278.

[10] J. A. Pople, *J. Chem. Phys.* **1991**, *95*, 4385–4388.

[11] a) D. Sellmann, K. Jödden, *Angew. Chem.* **1977**, *89*, 480–482; *Angew. Chem. Int. Ed. Engl.* **1977**, *16*, 464–465; b) D. Sellmann, R. Gerlach, K. Jödden, *J. Organomet. Chem.* **1979**, *178*, 433–447.

[12] For $[(OC)_5Cr-N_2H_2-Mn(CO)_2Cp]$, see ref. [11]; for $[M(N_2H_2)(CO)_2(PPh_3)_2Br]SO_3CF_3$ (M = Ru, Os), see: a) G. L. Hillhouse, T.-Y. Chen, A. Ponce, A. L. Rheingold, *Angew. Chem.* **1994**, *106*, 703–705; *Angew. Chem. Int. Ed. Engl.* **1994**, *33*, 657–659; b) G. L. Hillhouse, M. R. Smith III, T.-Y. Chen, *J. Am. Chem. Soc.* **1993**, *115*, 8638–8642.

[13] a) D. Sellmann, J. Sutter, *Acc. Chem. Res.* **1997**, *30*, 460–469; b) M. Reiher, O. Salomon, D. Sellmann, B. A. Hess, *Chem. Eur. J.* **2001**, *7*, 5195–5202.

[14] D. Sellmann, D. C. F. Blum, F. W. Heinemann, *Inorg. Chim. Acta* **2002**, *337*, 1–10.

[15] K. R. Barnard, M. Bruck, S. Huber, C. Grittini, J. H. Enemark, R. W. Gable, A. G. Wedd, *Inorg. Chem.* **1997**, *36*, 637–649.

[16] S. Sekusak, G. Frenking, *J. Mol. Struct.* **2001**, *17*, 541–549.

[17] a) D. Sellmann, E. Böhlen, M. Waeber, G. Huttner, L. Zsolnai, *Angew. Chem.* **1985**, *97*, 984–985; *Angew. Chem. Int. Ed. Engl.* **1985**, *24*, 981–982; b) D. Sellmann, J. Käppler, F. Knoch, M. Moll, *Inorg. Chem.* **1993**, *32*, 960–964.

[18] T. Gottschalk-Gaudig, Dissertation, University of Erlangen-Nuremberg, **1997**.

[19] a) D. Sellmann, K. Engl, F. W. Heinemann, J. Sieler, *Eur. J. Inorg. Chem.* **2000**, 1079–1098; b) D. Sellmann, T. Gottschalk-Gaudig, K. Engl, F. W. Heinemann, *Eur. J. Inorg. Chem.* **1999**, 333–339.

[20] a) A. D. Becke, *Phys. Rev. A* **1988**, *38*, 3098–3100; b) J. P. Perdew, *Phys. Rev. B* **1986**, *33*, 8822–8824.

[21] A. Schäfer, H. Horn, R. Ahlrichs, *J. Chem. Phys.* **1992**, *97*, 2571–2577.
[22] D. Sellmann, A. Hennige, F. W. Heinemann, *Inorg. Chim. Acta* **1998**, *280*, 39–49.
[23] J. Thiele, *Liebigs Ann. Chem.* **1882**, *271*, 127.
[24] A. C. T. North, D. C. Phillips, F. S. Mathews, *Acta Cryst. A* **1968**, *24*, 351–359.
[25] R. H. Blessing, *Acta Cryst. A* **1995**, *51*, 33–38.
[26] SADABS, Bruker-AXS, Inc., Madison, WI, USA, **2002**.
[27] R. Ahlrichs, M. Bär, M. Häser, H. Horn, C. Kölmel, *Chem. Phys. Lett.* **1989**, *162*, 165–169.
[28] K. Eichkorn, O. Treutler, H. Öhm, M. Häser, R. Ahlrichs, *Chem. Phys. Lett.* **1995**, *240*, 383–390.
[29] K. Eichkorn, F. Weigend, O. Treutler, R. Ahlrichs, *Prog. Theor. Chem. Phys.* **1997**, *97*, 119–124.

Received: September 1, 2003 [F5499]